Imaging windows for long-term intravital imaging
General overview and technical insights

Maria Alieva[1,†], Laila Ritsma[2,3,†], Randy J Giedt[4], Ralph Weissleder[4,5], and Jacco van Rheenen[1,*]

[1]Cancer Genomics Netherlands; Hubrecht Institute-KNAW and University Medical Centre Utrecht; CT Utrecht, The Netherlands; [2]Center for Cancer Research and Center for Regenerative Medicine; Massachusetts General Hospital; Richard B. Simches Research Center; Harvard Medical School; Boston, MA USA; [3]Broad Institute of Harvard and Massachusetts Institute for Technology; Cambridge, MA USA; [4]Center for Systems Biology; Massachusetts General Hospital; Richard B. Simches Research Center; Harvard Medical School; Boston, MA USA; [5]Department of Systems Biology; Harvard Medical School; Boston, MA USA

[†]These authors contributed equally to this work.

Intravital microscopy is increasingly used to visualize and quantitate dynamic biological processes at the (sub)cellular level in live animals. By visualizing tissues through imaging windows, individual cells (e.g., cancer, host, or stem cells) can be tracked and studied over a time-span of days to months. Several imaging windows have been developed to access tissues including the brain, superficial fascia, mammary glands, liver, kidney, pancreas, and small intestine among others. Here, we review the development of imaging windows and compare the most commonly used long-term imaging windows for cancer biology: the cranial imaging window, the dorsal skin fold chamber, the mammary imaging window, and the abdominal imaging window. Moreover, we provide technical details, considerations, and trouble-shooting tips on the surgical procedures and microscopy setups for each imaging window and explain different strategies to assure imaging of the same area over multiple imaging sessions. This review aims to be a useful resource for establishing the long-term intravital imaging procedure.

Introduction

Intravital microscopy (IVM) is a well-established technique by which tissues can be imaged at (sub)cellular resolution in living animals.[1] By visualizing various cell types, non-cellular structural factors (extracellular matrix), fluorescently-tagged proteins or fluorescent biosensors over time, many dynamic (patho)physiological processes can be investigated.[2-5] For example, intravital imaging of fluorescent glioma brain tumors uncovers that individual cells migrate along blood vessels (**Fig. 1A**). To gain imaging access to tissues deep inside animals such as orthotopic cancers of the breast, brain and liver,

imaging sites can be surgically exposed.[6-8] However, this technique is not conductive to repetitive imaging, and even when animal vitals are tightly measured and controlled surgical IVM can only be performed up to 40 h.[6] To extend imaging over days or months, several imaging windows have been developed (**Fig. 2**). By utilizing imaging windows, animals can recover from anesthesia in between the imaging sessions and tissues can be visualized up to a year, so that processes such as tumor growth become visible at cellular resolution (**Fig. 1B**).[9-12] In this technical resource, we will review various imaging windows used for cancer research, and provide technical details, considerations, and trouble-shooting tips.

Introduction of Imaging Windows

Already in the early 19th century, the first reports on cranial imaging windows (CIW) appeared. In 1811 a physician in Italy inserted a wooden cylinder topped with a watch glass in the skull of a dog to study brain motions caused by intrathoracic pressure.[13] Since then, several others contributed significantly to the establishment of the CIW, such as Donders, who eliminated the air in between the window and brain by administering fluid as the window was pressed into place.[14] In 1928, Forbes published a CIW method in which he describes the complete immobilization of the skull and the insertion of an air-tight window with relatively normal intracranial pressure to gain imaging access to brain tissue to visualize pia mater blood vessels.[15] Since that time this imaging window has been widely used to study neocortical plasticity and structure,[16,17] cerebral circulation,[18] and pathological processes that take place in the brain such as ischemic stroke,[19] injury,[20] degenerative disease,[21] and cancer.[22]

To visualize skin tissue, Algire developed the dorsal skinfold chamber (DSC) by adapting earlier "transparent-chamber techniques" from the rabbit ear and skin to mice.[23,24] The chamber has proven popular for studying various processes including microcirculation,[25] tumor growth,[26] angiogenesis,[27] and ischemic reperfusion.[28] More recently, the mammary imaging window
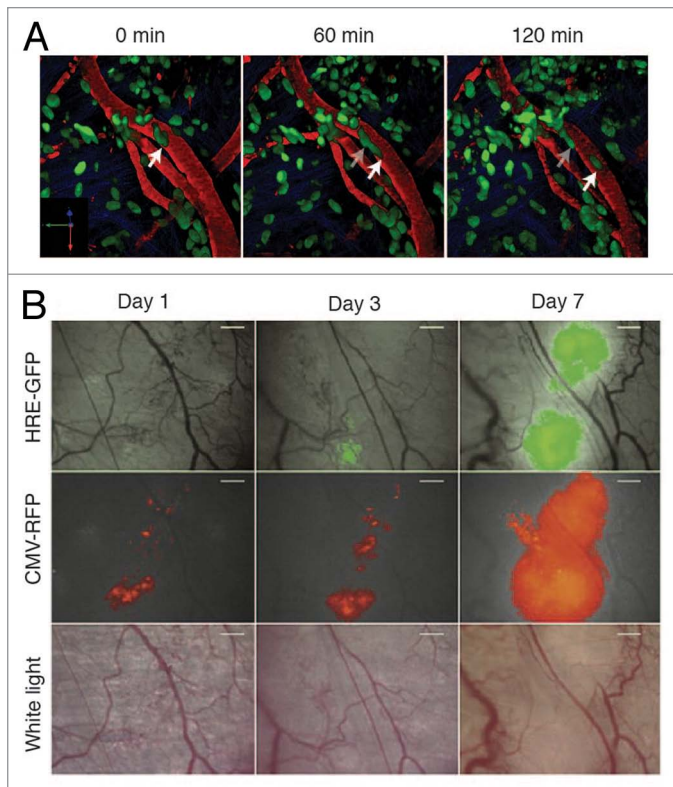
Figure 1. Intravital microscopy of tumors through imaging windows. (**A**) A 3D reconstruction of a murine orthotopic glioma (GL261-H2B Dendra2). The time-series show single cells migrating along the vessels. Nuclear localization of the photoprotein allows accurate single cell tracking. Green: tumor cell nuclei; Red: Dextran-labeled vasculature. Scale bar, 12 μm. (**B**) 4T1 tumor cell growth was visualized at day 1, 3 and 7 following tumor implantation through the dorsal skinfold chamber. A HIF-1 reporter (HRE-GFP) was expressed in tumor cells (CMV-RFP) and both were visualized using fluorescence microscopy. The vasculature is shown in red and was visualized using white light. Scale bar, 300 μm. Reprinted from reference 102 with permission from Elsevier.

(MIW) was developed to visualize breast tissues and tumors.[29,30] Importantly, the MIW was the first imaging window that allowed for the study of genetically driven tumors that recapitulate the progression of human mammary carcinomas[11] in addition to more conventional xenograft tumor models.[29] To visualize abdominal organs like the small intestine, kidney, spleen, pancreas and liver, the abdominal imaging window (AIW) was developed.[31,32] In recent studies we have used the AIW to study intestinal stem cell homeostasis,[12] as well as how colorectal cancer cells colonize the liver and form metastases.[32] In addition to the MIW and AIW, two groups developed a spinal cord imaging window to study cellular dynamics and regeneration after spinal cord injury.[33,34] Moreover, to study immune cell motility and response to infection, imaging chambers for lungs have been developed.[35,36] However, in contrast to all other imaging windows, the lung imaging windows do not allow for repeated imaging and are not suited for long-term (>1 d) studies.[35,36] In this manuscript, we will focus on the imaging windows that are frequently used for long-term cancer studies: the CIW, DSC, MIW, and AIW (**Fig. 2**).

General Considerations for Surgical Implantation of Imaging Windows

When surgically implanting imaging windows, several general surgical aspects must be taken into account including maintenance and control of vital parameters, analgesia, anesthesia, and post-operative care. Inaccurate use of each of these techniques may result in death, severe pain, or failure of the surgical procedure, and are therefore of critical importance. Below, we will discuss each surgical aspect in detail.

Pre and peri-operative care

In humans it is common for patients to fast before undergoing surgery to prevent food or liquid from being vomited and aspirated into the lungs. Rodents are incapable of vomiting, thus eliminating the need to fast them.[37] We recommend shaving and depilating the mouse prior to surgery, and applying a betadine scrub. This decreases the chance of infections caused by bacterial flora on skin and hair remnants. Moreover, it is recommended to work in an aseptic environment to avoid infections, which can cause failure of CIW experiments.[16,38] Furthermore, surgical tools and imaging windows must be sterilized (for example, by an autoclave/hot bead sterilizer) or disinfected (immersion into 70% ethanol).[31,39] To reduce the chance of inflammation and cell attachment (including immune cells), the coverslip can be coated with PEG (polyethylene glycol).[31]

Vital parameters

Hypo and hyperthermia can cause death during surgery.[40] At room temperature, a mouse can lose 1 degree of body temperature every 5 min, so regulation and monitoring of temperature during surgery is essential. Ideally, body temperature should be maintained near 37 °C, which can be accomplished by the use of a heat pad or lamp.[6,41] A heat pad with adjustable temperature is advisable (**Tables 1 and 2**). In case of a non-adjustable heat pad, filter papers or tissues placed between the heat pad and the animal may help to control the body temperature of the mouse. To monitor body temperature during surgery, the use of a rectal probe is recommended. Besides body temperature, other vital parameters can be monitored using non-invasive monitors like the MouseOx Plus (**Tables 1 and 2**). This equipment is specifically designed to probe vital signs in small rodents and provides measurements of the arterial oxygen saturation, heart and respiratory rate, temperature, and pulse and breathing distention.[42]

Anesthetics and analgesics

Anesthetics are used to sedate animals and analgesics are used to relieve animals from pain. Anesthetics can either be inhaled or injected, whereas analgesics are usually injected. The choice of an anesthetic and analgesic method is determined by several parameters: the type of surgery to be performed, the depth of anesthesia, and the extent and ease of the procedure. Furthermore, depending on the type of experiment to be performed, certain anesthetic or analgesics might cause unfavorable side effects. For example, isoflurane has been shown to induce cerebral vasodilation whereas ketamine causes vasoconstriction and increases cerebral blood flow.[43-45] These effects should be evaluated if important for the experimental setup.
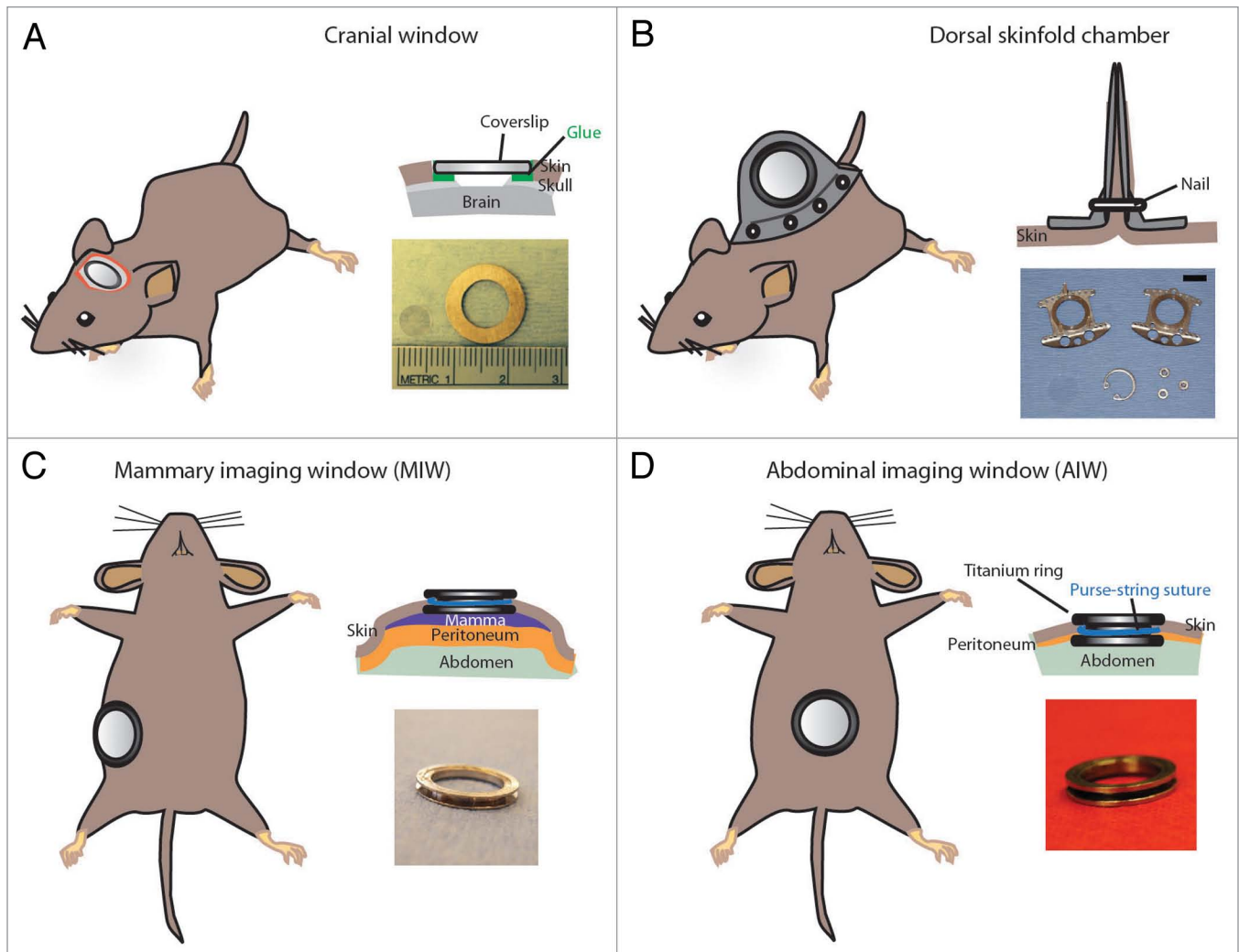
Figure 2. Most frequently used imaging windows in cancer research. (**A**) The CIW: the coverslip is glued onto the skull. The image depicts a coverslip and a metal ring. (**B**) The DSC: the metal frame of the window is clamped around the dorsal skinfold. Photograph shows the window chamber, retaining nuts and glass window. Scale bar, 1 cm. Photograph reprinted from reference 39 by permission from Macmillan Publishers Ltd: Nature Protocols. (**C**) The MIW: a purse-string suture tightens the skin around the MIW. The photograph depicts the titanium MIW. (**D**) The AIW: a purse-string suture secures the AIW onto the abdominal wall and skin. The photograph depicts the titanium AIW with the groove in the side and is adapted from reference 32. All cartoons from reference 32, reprinted with permission from AAAS.

Isoflurane is a widely used inhalation anesthetic for rodent surgery and the first choice over injectable anesthetics[31] due to a fast induction and recovery, good control over anesthesia depth and length, and minimal impact on hemodynamics.[37,46,47] Isoflurane requires oxygen as a carrier and the dose used for maintenance varies from 0.5 to 3% (vol/vol) in O_2.[8,48-50] Note that the actual dose varies depending on the equipment and animal strain, sex, age, and condition. The depth of anesthesia is adequate when the palpebral reflexes are absent and the animal is unresponsive to external stimuli such as a toe pinch. A constant heart and respiratory rate is important, and gasping (agonal) respiration should be prevented.[37,51] At rest, mice have an average respiratory rate of 180 breaths per minute. During anesthesia, a reduction of over 50% in respiratory rate is expected, and a breath rate between 50 and 100 breaths per minute is acceptable for mice.[52] Isoflurane has been successfully used to surgically implant the MIW, AIW, and DSC.[11,31] This anesthetic has also been used for CIW surgery,[53] however, it has been reported that it can intensify dura mater bleeding during the operation (**Table 2**).[16] Additionally, the use of an inhalation mask restricts the handling of the animal and makes head fixation on the stereotactic frame more challenging.

Ketamine/Xylazine combinations are widely used as injectable anesthetics for surgical procedures at concentrations varying from 80 to 100 mg/kg for Ketamine and 5 to 10 mg/kg for Xylazine. The recommended dose for imaging window surgery of Ketamine (100 mg/kg) and Xylazine (10 mg/kg) induces a surgical plane for about half an hour.[16] Cardiovascular depression and ketamine irritancy due to low pH are the main disadvantages of this combination.[54] For surgeries that require a long time (>1.5hr) such as CIW, the combination of Hypnorm (Fluanison [neuroleptic] + Fentanyl [opioid]) (0.4 ml/kg) +

Table 1. Window surgery equipment

Equipment	Company	Product	Window
Anesthetics scavenger	VET tech solutions LTD OR Harvard Apparatus	Active scavenger unit Fluovac	GEN GEN
Antiseptic surgical scrub	Betadine	Betasept Antiseptic Surgical Scrub	GEN
Balance	Denver Instruments	Multiple available	DSC
Buprenorphine hydrochloride	BD pharmaceuticals limited	Temgesic (0.3 mg/ml)	GEN
Clipper	Wella	Contura clipper	GEN
Cover glass	Warner Instruments VWK international Thermo Scientific	Small Diameter Coverglass (5mm, #1) Coverslips round 6 mm Menzel Glazer 12 mm	DSC CIW MIW, AIW
Cyanoacrylate glue	Henkel	Pattex Ultra Gel	CIW, AIW
Dental cement	Vertex dental	Vertex Self-Curing	CIW
Drill	Dremel	Dremel 3000 (dental drill may be more convenient) + 105 Engraving Cutter	CIW
Forceps	Roboz surgical instruments Co Neolab-DUMONT	Graefe forceps curved, serrated Forceps No. 5, smooth tying platform	GEN GEN
Heating pad	Inventum Holland VB		GEN
Hypnorm	VetaPharma Ltd	Hypnorm (Fentanyl citrate 0,315mg/ml+ Fluanison 10mg/ml)	CIW
Induction cage	Techniplast	Induction cage with autoclavable filter top	GEN
Inhalation anesthetic	Abbott OR Baxter	Isoflurane (100% w/w solution) Forane, Liquid for inhalation	GEN
Isoflurane Vaporizer	Isotec OR Vet Tech solutions LTD	Anesthetics machine	GEN
Midazolam	Actavis	Midazolam Actavis 5mg/ml	CIW
Needle	BD microlance	16 gauge needle	DSC
Needle holder	Aesculap		GEN
Opthalmic ointment	Kela Veterinaria	Duodrops veter kela 10 ml	GEN
Scissors	Roboz surgical instruments Co	Microdissection scissors 3.5 inch	GEN
Silicone oil	Sigma- Aldrich	Silicone oil	CIW
Stereotaxic frame	Stoelting	Lab standard™ stereotaxic, rat and mouse	CIW
Sterile surgical gloves	SemperMed		GEN
Sterilizer	Cell point Scientific	Germinator 500	GEN
Surgery light	Schott	Ace I	DSC
Surgical drape	Medline industries		GEN
Surgical stereo microscope	Olympus		DSC, CIW
Sutures	Ethilon/Ethicon	Polypropylene sutures (4.0)	DSC, MIW, AIW
Vital sign monitors	Starr Life Sciences Corp.	MouseOx Plus	GEN
Window (chamber) frame	FMI instrumed AJP Trading Co. INC	Titanium AIW or MIW: STMF136–02A that meets ISO5832 part 3 and EN10204–3.1.B Window chamber, C-holder, screws, retaining ring	MIW, AIW DSC

The window column indicates for which type of surgery the equipment is used: DSC, CIW, MIW, AIW or GEN (general equipment for all surgeries).

Midazolam (benzodiazepine sedative) (2 mg/kg) (**Table 1**) at a dose of 1:1:2 in sterile water is advised. This anesthetic supplies deep sedation for up to 4 h, which can be reverted by the injection of 100 μg/kg of buprenorphine (**Table 1**).

For each anesthetic alternative, an adequate analgesic drug should be supplied. Subcutaneous or intramuscular administration of an opioid analgesic such as buprenorphine (100 μg/kg) prior to the operation is recommended for mice under inhalation anesthesia. Ketamine/Xylazine and Hypnorm/Midazolam cocktails already contain an analgesic component that exerts its effect during the surgery. Post-operative administration of buprenorphine will provide additional pain relief for

Table 2. Troubleshooting imaging window surgeries

Problem	Possible reason	Solution DSC	Solution MIW	Solution AIW	Solution CIW
Mouse dies during surgery	Hypo/Hyperthermia	Control the power of the heating pad and measure mouse temperature.			Control the power of the heating pad and measure mouse temperature.
	Excessive anesthesia	Reduce the amount of anesthesia.			Adjust the amount of anesthesia per mouse weight.
Bleeding during drilling and dura mater removal	Vascular damage	NA			Control the bleeding by the Gelfoam sponge. Precisely perform these procedures under a stereomicroscope.
The window falls out	The suture was placed too close to the skin edge.	NA	Mouse needs to be sacrificed because the tissue underneath the window is most likely dehydrated.		NA
	The dental cement was applied on the skin		NA		Glue the skin and apply the dental cement on the skull.
Bleeding underneath the coverslip	Vascular damage	Be more careful during surgery; cauterize wound.	Remove the liquid under the window as indicated above (**Table 4**). Be more careful during surgery; cauterize wound.		
The mouse head moves	The mouse head is not properly fixed on the stereotactic frame.	NA			Ensure that the mouse head is firmly fixed by ear bars and a teeth holder.
The abdominal organ moves underneath the window	Too little glue was used to fix the organ to the window.	NA		Wait a day. Sometimes organ settling takes about 24 h.	NA
				Use gels like CyGel to reduce organ movement.[12]	
			Take out the window by cutting the stitch and place it again.		
There is an infection underneath the window (white cloudy liquid)	No aseptic working environment was maintained or the instruments were not sterile.	Euthanize the mouse. Next time provide antibiotics.			

NA indicates not applicable.

up to 12 h. As mentioned above, buprenorphine is an antagonist of Hypnorm and speeds its reversion, thus it should not be used as a preoperative analgesic in combination with Hypnorm/Dormicum. The use of a topical or subcutaneous local analgesic such as Xylocaine (1%) at the incision site will provide additional pain relief.

Post-operative care

Following surgery, it is necessary to monitor the animal for pain and discomfort (**Table 3**). If needed, an additional dose of buprenorphine can be supplied. Other anti-inflammatory drugs such as Carprofen (5 mg/Kg) or Dexamethasone (0.2 mg/Kg) are often supplied to prevent inflammation and brain swelling when performing a CIW.[16,38,55] However, it is important to realize that suppression of the immune system, for example by reduced immune cell infiltration,[56,57] can affect important study parameters. For instance, immune cell infiltration has been shown to be involved in neoplastic progression and migration.[58,59] Additionally, analgesic drugs can affect the neoplastic microenvironment, particularly macrophages infiltration and angiogenesis.[60,61] In the case of the DSC it is key to provide the mice with antibiotics (sulfamethoxazole and Trimethoprim [95 mg/kg Sulfatrim] or similar) in their drinking water because it reduces possible bacterial-induced inflammatory responses.[62-65] To prevent complications in long-term studies, antibiotics can also be administered for the CIW. After the surgery, it is important to house the mice solitarily to avoid window damage or detachment. A warm, dry and quiet environment is recommended to reduce hypoxemia and shivering. Also, in case of severely anesthetized animals, an oxygen-enriched atmosphere and intraperitoneal or subcutaneous fluid therapy may support a faster recovery. Administration of a maximum of 0.6 mL of 0.9% saline solution in the subcutaneous space of a mouse every half a day can prevent

Table 3. Clinical parameters of distress

Parameter	Signs	Cause
Activity level	Hypo activity (hunched, lethargic), hyperactivity, restlessness, lack of curiosity.	Pain.
Attitude	No awareness of surroundings.	Depression, pain.
Behavior, spontaneous	Squealing, self-trauma, isolation from cage mates.	Pain.
Behavior, Provoked	Vocalization, teeth grinding, struggling, hiding, aggressiveness, unwilling to move, guarding the incision site.	Pain.
Body Condition	Tenting of the skin, missing anatomy, dehydration, anorexia, absence of feces and urine.	Reduced food and fluid intake.
Fur and skin	Ruffled or greasy or dull fur, porphyrin (red) staining around eyes and nose, cyanotic or pale ears, feet, tail, skin lesions, soiled anal or genital area. Redness and swelling at incision site.	Failure to groom. Excessive licking/scratching. Pain. Infection.
Extremities	Cold, blue, hot or red.	Hypo or hyperthermia.
Eyes	Clarity/condition of lens, sunken or protruding eyes.	Pain. Failure to groom.
Posture	Hunched back, tucked abdomen, head tucked down.	Pain.
Locomotion	Lameness, favoring a limb, upright or downwards.	Pain, physical blockade.
Neurological	Tremor, convulsion, weakness, circling, paralysis, head tilt, coma.	Neurological trauma.
Vital Signs	Respiratory distress (open mouth breathing, agonal breathing, pronounced chest movement).	Shortage of oxygen. Pain.

dehydration.[37] The animal should be monitored for discomfort by visual examination of behavior, appearance and weight at least twice per week (**Table 3**).

Considerations for each imaging window

The four window implantations discussed in this article consist of a coverslip inserted in a metal frame that protects and gives optical access to the tissue of interest (**Fig. 2**). Titanium has been the metal of choice for the frame due to its biocompatibility.[66] High-grade stainless steel is less bio-compatible[66] but is a less expensive alternative for titanium when the frame of the imaging window is not adhered directly to any tissue. The anatomical position of every imaging window requires a different method of fixation to the mouse. In contrast to other optical windows, the chronic CIW uses skull bone as a rigid support to fix the position of the coverslip (**Fig. 2A**). This solid support allows the acquisition of high quality images of the brain for up to a year.[67] This is in contrast to other tissues where there is no bone available for chamber fixation and chambers are therefore fixed to soft tissues such as the skin. These frames result in a higher failure probability due to detachment from their anchor points. Consequently, the time that DSC, MIW and AIW can be used for imaging is often limited to a few weeks. Below we explain the particulars of each window, include a surgical guide and provide a table that lists the equipment and equipment vendors (**Table 1**).

CIW

Two different CIWs are available: the chronic CIW and the thinned skull window. For the chronic CIW, the brain is exposed through a craniotomy and covered with a coverslip that is glued onto the skull. By contrast, for the thinned skull window, a microdrilled-thinned skull provides optical access to the brain surface without the requirement of implanting a cover glass, thus avoiding intracranial microenvironment alteration.[17] However, imaging through the thinned skull window is usually limited to a certain number of sessions due to bone regrowth and the necessity

of thinning the skull before each session. Despite mitigation of this issue by the reinforced thinned skull approach, light absorption by bone tissue nevertheless compromises imaging resolution and depth.[68] When selecting a CIW approach, it is important to realize that each type of window affects the brain's plasticity and microenvironment differently, potentially altering experimental outcomes.[69] Xu and colleagues compared the thinned skull and chronic CIW and showed that the latter induces an increase in dendritic spine turnover, microglia and astrocyte activation up to 1 month after imaging window surgery.[70] Keeping this in mind, the chronic CIW described in this article is a powerful tool for long-term studies[71,72] and when access to the brain is required.[10,73]

The window size varies from 5 to 7 mm in diameter and can be placed on the frontal or occipital lobe depending of the region of interest. To start the procedure, sedate the mouse by i.p. injection of Hypnorm (Fluanison [neuroleptic] + Fentanyl [opioid]) (0.4 ml/kg) + Midazolam (benzodiazepine sedative) (2 mg/kg) at a dose of 1:1:2 in sterile water (**Table 1**). After ensuring by toe pinches that the animal is fully unconscious, mount it in a stereotactic frame and secure the head using a nose clamp and two ear bars (**Fig. 3A**). Use a heating lamp to maintain the animal temperature during the procedure. Apply eye ointment in order to prevent the animal's eyes from drying out (**Table 1**). Shave the top part of the head and apply a drop of Xylocaine (Lidocaine 1% + Epinerphine 1:100,000) solution to further prevent pain. Perform a longitudinal incision of the skin between the occiput and forehead and cut the skin in a circular manner on top of the skull (**Fig. 3B**). Scrape the periosteum underneath and apply a drop of Xylocaine to further prevent pain. Using a high-speed drill (**Table 1**), slowly and carefully perform a 5-mm circle groove over the region of interest (**Fig. 3C and D**). To avoid brain overheating apply cold sterile cortex buffer (125 mM NaCl, 5 mM KCl, 10 mM glucose, 10 mM HEPES buffer, 2 mM $MgSO_4$, and 2 mM $CaCl_2$, pH 7.4) during the drilling process (**Fig. 3E**). When

the bone flap becomes loose, gently lift it under a drop of cortex buffer (**Fig. 3F**). The buffer is important to avoid brain dehydration and bleeding of the dura mater. The exposed cortical surface must continuously be kept moist with cortex buffer. To improve imaging resolution the dura mater can be removed with thin forceps (**Table 1**). This step is necessary when superficial injection is performed since the dura is a very elastic membrane. The use of a surgical stereo microscope (**Table 1**) is recommended during drilling and dura mater removal (**Fig. 3D–F**). Accuracy is critical to avoid bleeding and brain damage (**Table 2**). At this point any tissue manipulations such as cell or dye injections required for the experimental setup can be performed. To conclude the procedure, seal the exposed brain with silicone oil, glue a 6-mm coverslip (**Tables 1 and 4**) on top and apply dental acrylic cement (**Table 1**) on the skull surface, covering the edge of the coverslip (**Fig. 3G**). In order to attach the mouse to the microscope during imaging a fixation system should be secured on the top of the head. The fixation can be achieved by the insertion in the dental cement of a bar or a ring (around the window) that will be attached to the microscope by means of screws or magnets (**Fig. 3H**). A light metal such as titanium or steel should be used for animal comfort. After surgery the animal should be placed on a heating pad (37 °C) until it recovers from the anesthesia (**Table 1**). A single dose of 100 μg/kg of buprenorphine (**Table 1**) should be administered to prevent pain and speed the recovery (**Fig. 3I**).

DSC

The DSC is one of the most widely used imaging windows in cancer biology. The window consists of two large metal frames that fix the dorsal skin tightly together (**Fig. 2B**; **Table 1**).[73] The frames are attached to one another using screws and sutures,[74] ensuring a stable fixation of the tissue within the chamber. The relative small depth within the chamber allows easy access to microvasculature and implanted tumors, which facilitates imaging at great detail. Note that in this display tumor growth and interaction with the stroma varies upon injection method. Cell implantation between the dermis and the coverslip will cause quasi two-dimensional growth. To recapitulate the interaction of the tumor with the surrounding tissue cells should be injected directly in the deep dermis.[26,75] Because the DSC is located on the exterior of the animal body, movement due to respiration is restrained as compared with other chambers and can be nearly eliminated via mechanically securing the chamber during imaging. However, the location of the chamber outside of the animal's body has the disadvantage that normal body temperature within the window is not maintained when the mouse is kept at optimal housing temperature (varying from 20 to 26 °C for individual and group housing).[74,76] The reduced temperature in the DSC, along with other factors, is one reason that some slow growing tumor models do not form tumors within the DSC.[77] To enhance xenograft tumor formation, several improvements to the DSC have been proposed. By letting BxPC-3 cells form a tumor before DSC implantation it was shown that tumors were formed in DSCs, where these cells were previously unsuccessful.[77] Other methods to increase tumor growth in the DSC are the use of matrigel during tumor cell injection, implantation of tumor
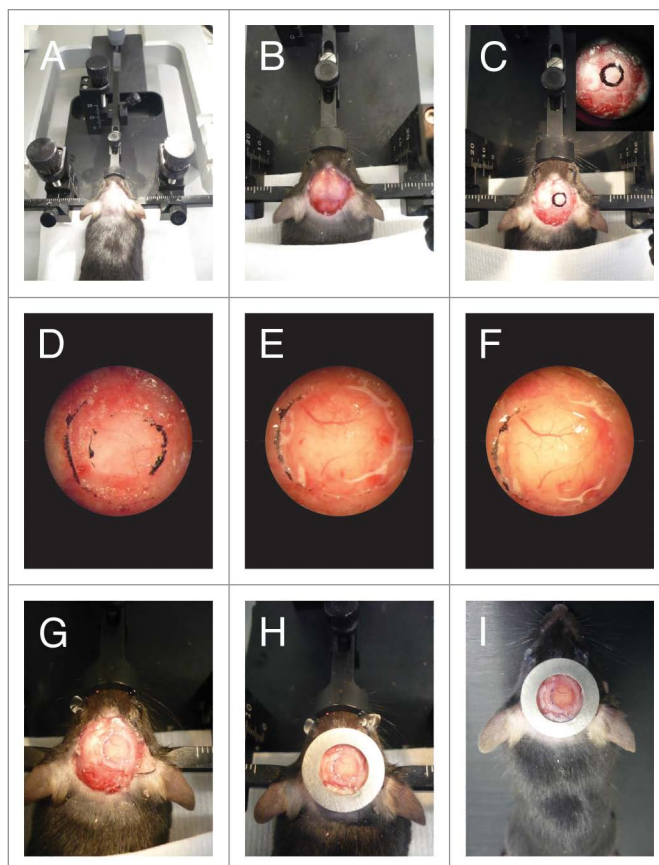
Figure 3. CIW surgery. (**A**) The mouse head is shaved and fixed on a stereotaxic frame. (**B**) The skin is cut in a circular manner around the skull and the periosteum is scraped. (**C**) 5mm diameter circle is drawn around the region of interest. (**D**) A groove is drilled around the region of interest. (**E**) Cold cortex buffer is applied during drilling. (**F**) The craniotomy is lifted under a drop of saline exposing the brain. (**G**) The brain is covered with silicone oil and sealed with a 6 mm diameter coverslip. (**H**) Dental cement is applied to cover exposed skull and a stainless steel ring is glued parallel to the coverslip. (**I**) The mouse is injected with 100 μg/kg of buprenorphine and allowed to recover on a heating pad.

pieces instead of (dissociated) tumor cells, co-implantation of tumor cells and healthy orthotopic tissue, and housing animals in warm temperatures (33–34 °C).[41,74,78]

To implant the window chamber begin by sedating the animal using isoflurane (0.5–3% in O$_2$) or other anesthetics outlined above (**Table 1**). Sufficient analgesic (buprenorphine, ip [100 μg/kg]) (**Table 1**) should be provided at least half an hour before the start of the surgery, immediately following the procedure, and twice per day thereafter for 3 d. After sedation, shave (**Table 1**), depilate, and disinfect with Antiseptic Surgical Scrub or similar (**Table 1**) the dorsal area from the neck to hip. Apply eye ointment to prevent dehydration of the eyes (**Table 1**). Finally, before any surgical procedure is started, a toe-pinch or similar procedure to assess the state of the animal's sedation should be conducted.

To start the chamber implantation, position the anesthetized and shaven animal on a heating pad (37 °C) with a surgical light available (**Table 1**). To begin to fit the chamber, first stretch the dorsal skin in front of the surgical light and view the vasculature.

Table 4. Troubleshooting imaging

Problem	Possible reason	Solution DSC	Solution MIW	Solution AIW	Solution CIW
Poor visibility	Liquid accumulation or "membrane" formation can interfere with imaging.	Remove the O-ring and the coverslip to get access to the tissue. Use forceps or a cotton tip applicator to remove the membrane or liquid. Then replace the coverslip and O-ring.	Remove the liquid under the window by inserting a 25-G needle and slowly filling the syringe. Avoid hitting the organ or breaking the coverslip.		NA
	The tissue of interest is too far from the objective.	NA	If using an inverted microscope, wait for 30–45 min until the tissue gets closer to the objective by gravity.		
		NA	NA		Reduce the amount of silicone oil between the coverslip and the brain. The coverslip should be glued at the minimal distance from the brain.
The image is dark	When water objectives are used, the amount of water in between the objective and coverslip may be inadequate.	Supply water to the objective manually or use a dispenser that can regulate water supply automatically.			The use of an oil-immersion lens or a dry objective can be considered as well. However, often a trade-off must be made with a reduction in NA.
Bleeding under the coverslip	Vascular damage	Remove the liquid under the window as indicated above. If extensive bleeding is obstructing tumor visualization, bring mouse under anesthesia and break the window, remove the blood and place a new window.			If tumor is still visible take no action.
Mouse dies during imaging	Sedation is too deep.	Establish appropriate sedation level for your experiment. For long-term experiments a low amount of isoflurane is recommended. Control mouse breathing and maintain the temperature at 36°C. If breathing is irregular decrease the amount of isoflurane.			
	Mouse is hypo/hyperthermic and/or dehydrated	To avoid dehydration inject the animal with saline prior or during the imaging session. Maintain the temperature of the mouse at 36C using a heated blanket or a heated climate chamber that surrounds the microscope.			
Mouse/organ moves during the imaging	Sedation is inadequate. The mouse is not fully unconscious or is breathing irregularly.	NA	Establish appropriate sedation for your experiment.		
			Firmly fix the IW to the box with tape to avoid peristaltic movement or breathing artifacts.		
			Make use of a resonant scanner to increase the speed of image acquisition.		
			Use advanced motion compensation methods to reduce movements.[103,104]		
Tissue movement or deformation during imaging	Tissue is compressed if the mouse is imaged in a non-anatomical position. Eg. Brain imaged through a CIW on an inverted microscope	NA			Use image-processing software to correct the image deformation.

NA indicates not applicable.

By aligning the symmetrical vasculature in the light the animals longitudinal axis can be determined, which should be marked to allow for the chamber to be placed with an evenly distributed weight. Additional markings should be created along the transverse axis next to the peak of the animal back. These two lines will serve as guides for the correct placement of the window chamber. In order to implant the window chamber, it is next necessary to fan out the animal skin and secure the dorsal skin fold. This has been done in several ways in the past. One popular method is to suture a C-holder with 4–6 stitches, surgically stretching the skin (**Table 1**).[74] Another method utilizes clamps to pull and hold the skin in place.

The next step is to align the chamber. Typically, dorsal skin fold window chambers are made up of a front piece and a back piece, where the front piece is a thin metal section containing an area for the coverslip, and the back piece contains threads for screws (**Table 1**). To align the chamber, place the front piece on the skin fan so that the top of the chamber isn't too close to the top edge of the skin fold (to prevent skin tear and loss of the chamber) and the bottom isn't so close to the mouse body that

placing screws will penetrate the animal back muscle. When the chamber is properly aligned, use a 16 gauge needle (**Table 1**) or a hole punch to place holes cleanly through the animal's skin, ensuring that a hole is created by precisely puncturing the skin rather than tearing through it, the latter of which may decrease chamber life. Following this, the back piece of the chamber can then be attached and screwed or affixed into place depending on the specific chamber design in use. At this point place sutures (**Table 1**) on the upper edge of the window chamber to secure it in place. Careful attention should be paid to the tightness of the chamber attachment: if the chamber is too loose, infection or chamber failure could occur; too tight and blood circulation could be cut off, leading to tissue necrosis. After these sutures have been placed, the C-holder or other skin fold retaining method can be removed.

After chamber attachment, skin removal can be completed by using forceps (**Table 1**) to pull the skin away from the fascial tissue and cutting (**Table 1**) the circumference around the inner rim of the affixed window chamber. If necessary, tumor cell implantation can then be completed at this point by injecting 20–60 µl of cell suspension between the dermis and the fascia. The procedure is finished by placing a coverslip (**Table 1**) and securing it with a retaining ring.

Mice should be monitored both during recovery from anesthesia and post-surgically to ensure both animal health and tumor growth. Following the procedure, sulfamethoxazole and trimethoprim (95 mg/kg Sulfatrim) or similar antibiotics should be kept in the animal water supply to prevent infection (**Table 2**). Note that some antibiotics given alone or in combination with other drugs have been shown to affect tumor proliferation, angiogenesis, and metastasis and thus can affect the outcome of the experiment.[79,80] Generally tumors will be apparent within 5–15 days, depending on the cell line and mouse model. Prior to follow on imaging sessions retaining rings and coverslips can typically be removed and replaced with clean coverslips, allowing for optimal experimental imaging conditions.

Metal MIW

The anatomy and location of most inner organs does not allow for the relatively convenient skin squeezing and chamber attachment of the DSC, and therefore requires an alternative method of window fixation. For the MIW, the frame is sandwiched between the mammary gland and the skin and its position is fixed by glue and sutures perpendicular to the window.[81] To prevent detachment of the MIW, glue is applied to cover the sutures.[29] Others have used an adhesive bandage which covers the window for two days, or an Elizabethan collar adapted to protect the sutures.[30] The first reports of the MIW used non-reusable frames made from acryl or plastic (both bio-inert materials) with small holes for the sutures. However, recent studies used a metal MIW that is based on the AIW design that does not require such measures, and which displays a reduced risk of infection or window detachment as compared with the plastic MIWs.[11,32,82] The metal MIW consists of a titanium ring with a groove (0.9 mm for the MIW) (**Fig. 2C**; **Table 1**). A purse-string suture tightens the skin within the groove (**Figs. 2C and 4**). In contrast to the sutures in the plastic MIW, purse-string stitches are located within the groove
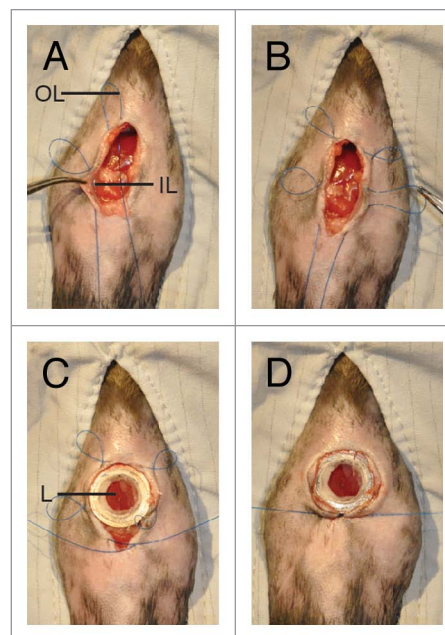
Figure 4. Purse-string suture fixes the AIW into the animal. (**A**) A purse-string suture is placed. The suture is first placed through skin and then through opposing abdominal wall. The outer loops (OL) are not tightened, whereas the inner loops (IL) are. (**B**) Once the purse-string suture is placed it should contain 4 or 5 outer loops. (**C**) The AIW is glued to the organ (liver [L]) and the skin and abdominal wall are placed within the window groove. (**D**) The sutures are tightened to secure the AIW in place. All pictures adapted from reference 31 by permission from Macmillan Publishers Ltd: Nature Protocols.

of the ring and do not need additional protection from biting (**Fig. 4**).[32]

The 4th mammary fat pad is the optimal location for inserting the mammary imaging window, since this location does not suffer from respiratory or motion artifacts. Before placing the window, anesthetize >8 wk old mice using isoflurane 0.5–3% in O_2 (**Table 1**). Ensure full sedation by a toe pinch, and place the animal on a heating pad (**Table 1**). Shave and depilate the area around the 4th mammary fat pad and disinfect using an alcohol swab. Apply eye ointment (**Table 1**) to prevent dehydration of the eyes. Fix the animal on its back with its legs and feet to the heating pad using tape, and make sure not to dislocate the joints. In case of insertion of the plastic MIW, use scissors (**Table 1**) to make a longitudinal incision of 10 mm and dissociate the subcutis from the cutis. Place the plastic ring in between the mammary gland and the skin, and suture (**Table 1**) the skin edge to the window using the holes. Close the wound by fusing the window to the skin edge using cyanoacrylate glue (**Table 1**), or use Neosporin ointment on the wound to prevent infection. If immediate imaging is not required, cover the wound with an adhesive bandage for up to two days. In case of implantation of the metal MIW, make a 12 mm anterior-posterior incision in the skin above the 4th mammary gland. Place a purse-string suture along the entire length of the incision, staying approximately 4 mm from the edge (**Fig. 4**; **Table 1**).[31] Insert the window on top of the mammary gland and place the skin in the window groove.
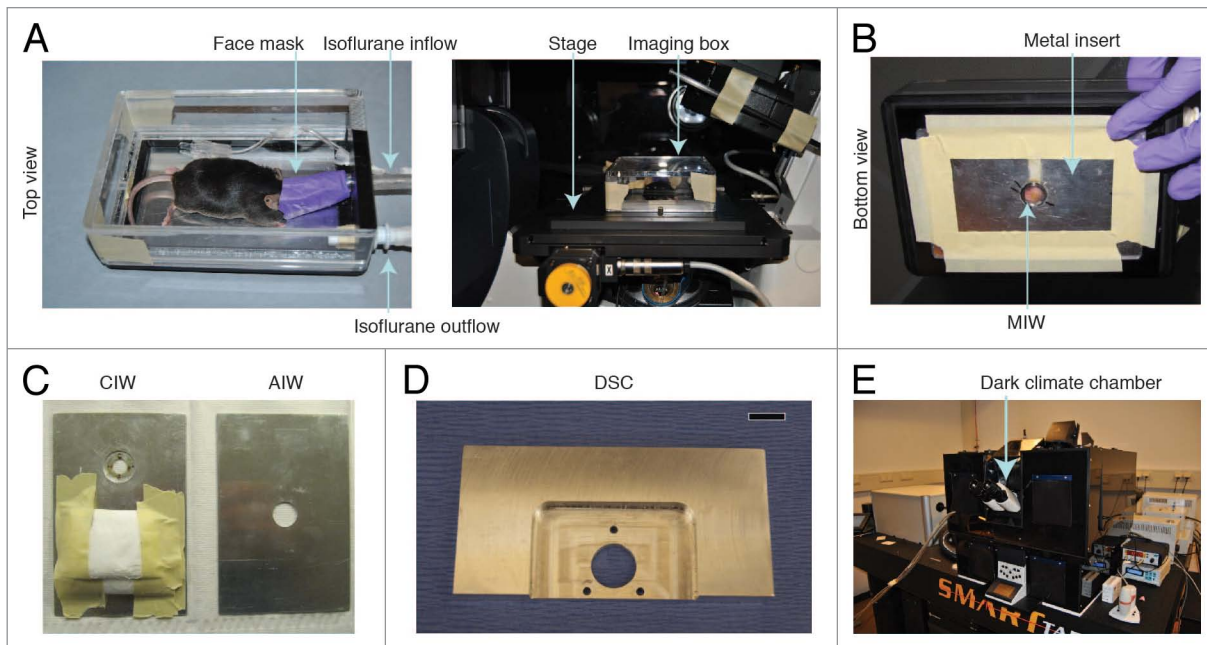
Figure 5. Fixation of the window during imaging. (**A**) A custom-designed imaging box that can be mounted on top of the stage of an inverted microscope. Reprinted from reference 31 by permission from Macmillan Publishers Ltd: Nature Protocols. (**B**) The imaging box shown from below. MIW is fixed in the center hole. (**C**) Inserts for the imaging box. A CIW window insert and an AIW insert are shown. (**D**) An imaging mount that can be used to fix a DSC onto a microscope stage. The three smaller holes allow the bolts on the window chamber to pass through and fix it, and the large hole permits imaging through the window. Scale bar, 1 cm. reprinted from reference 39 by permission from Mark W. Dewhirst and Macmillan Publishers Ltd: Nature Protocols. (**E**) An inverted Leica SP5 microscope with a dark climate chamber surrounding the stage is shown. Reprinted from reference 31 by permission from Macmillan Publishers Ltd: Nature Protocols.

Securely fix the window by tightening the suture and skin in the window groove, and make sure to "hide" the stitch underneath the upper ring (**Table 2**). After surgery the animals are placed on a heating pad (37 °C) (**Table 1**) until they recover from anesthesia.

AIW

Similar to the titanium MIW, the AIW is a ring with a groove on the side (1.3 mm for the AIW) (**Table 1**). A purse-string suture tightens the skin and abdominal wall within the groove (**Figs. 2C and 4**), leaving no direct opening to the abdomen, decreasing the danger of infection (**Fig. 4**).[31,32] However, since the organs move in the abdomen, for the AIW additional measures need to be taken (see below for details).

The AIW should preferably be inserted on the lateral side of the animal to prevent fluid accumulation of the abdomen behind the window. When the anatomical location of the organ of interest (e.g., liver) does not allow for insertion at the lateral side, it is important to completely cover the window by the organ so that the coverslip is sealed off from the abdomen. To implant the AIW, sedate the animal using isoflurane as described above. Provide sufficient analgesics (buprenorphine, 100 μg/kg i.p.) (**Table 1**) at least half an hour before the start of the surgery. Apply eye ointment to prevent dehydration of the eyes (**Table 1**). Shave (**Table 1**) and depilate the entire abdomen, and disinfect using an alcohol swab. Fix the animal on its back with its legs and feet to the heating pad using tape, and make sure not to dislocate the joints. As described above, the abdominal imaging window is similar to the

metal MIW and consists of a titanium ring with a groove in the middle (**Table 1**). Thus, follow the procedure described for the metal MIW up until the placement of the window. In this case, both the abdominal wall and the skin are placed in the groove, keeping the window secure (**Fig. 4**). To prevent organ movement and accumulation of fluids in between the window and organ, most organs are fixed to the window using tissue-fixatives such as cyanoacrylate glue (**Table 1**) or Vetbond tissue adhesive. Also, depending on the type of organ placed behind the AIW, additional surgical steps can be taken to minimize organ movement (**Table 2**) (for a detailed protocol, see ref. 31). After surgery the animals are placed on a heating pad (**Table 1**) until they recover from anesthesia. It can take up to 10 min for mice to fully recover. Post-operative monitoring and treatment of pain and possible infection is crucial for these animals.

Troubleshooting advice on IW surgeries is provided in **Table 2**.

Intravital Imaging through Imaging Windows

Fixation of the window during imaging

Several anesthetics can be used to sedate the animal for the imaging experiment. As discussed above, isoflurane is the preferred method since the duration and depth of the sedation can be precisely controlled (**Table 4**). When sedated by isoflurane (0.5–3% in O_2) (**Table 1**) and mounted on a microscope, mice can be imaged up to 40 h.[42] An upright microscope is often used
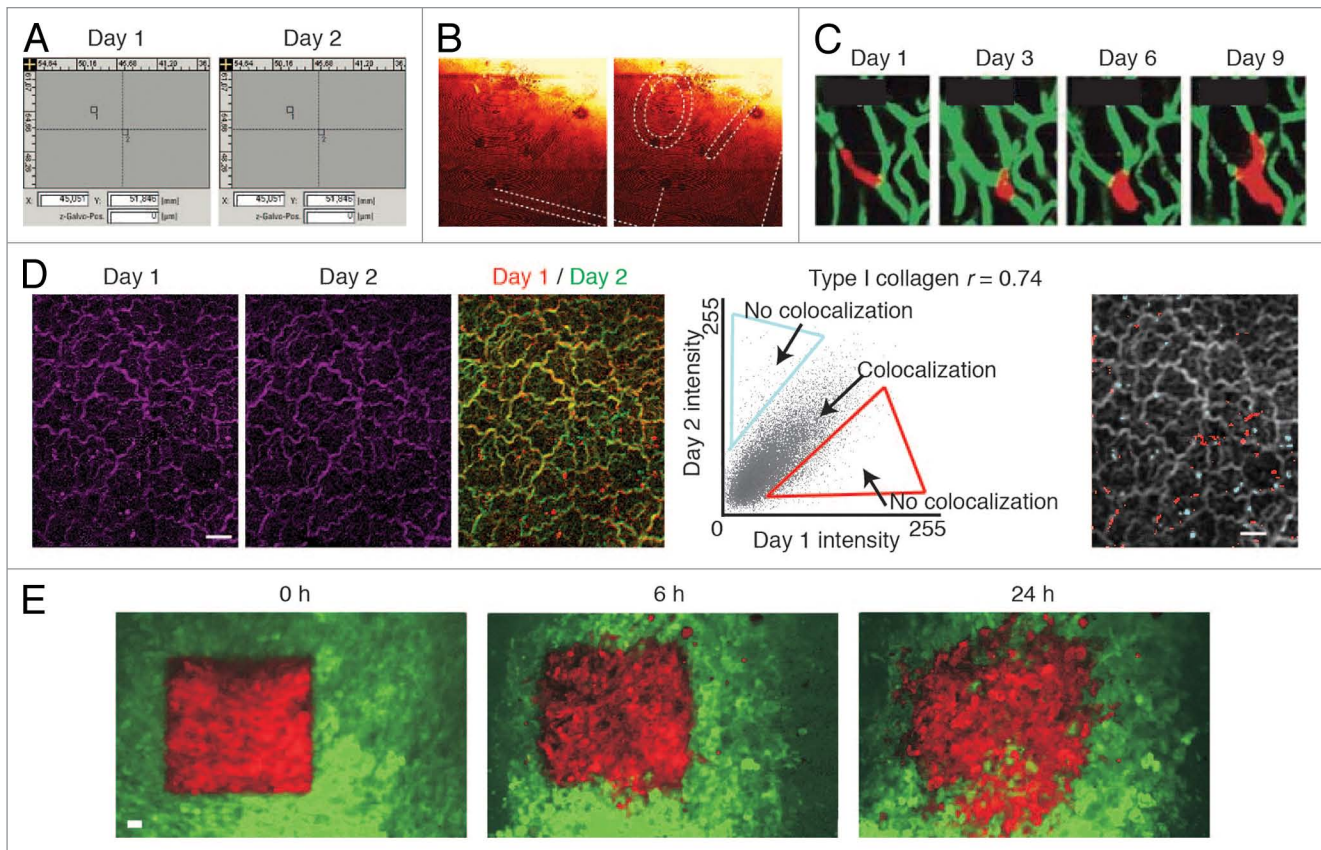
Figure 6. Retracing of the exact same field of view over multiple days. (**A**) A microscope with a motorized stage allows storage of regions of interest that can be imported at request. Reprinted from reference 12 by permission from Macmillan Publishers Ltd: Nature. (**B**) The numbered grids on a gridded cover glass can be visualized using reflection microscopy. The numbers can be used to retrace the same position over multiple days. Reprinted from reference 31 by permission from Macmillan Publishers Ltd: Nature. (**C**) The vasculature can be used as reference point to retrace a field of view. The microvasculature (green) is imaged through a cranial imaging window. Intravascular proliferation of injected PC14-PE6 lung carcinoma cells (red) can be seen from day 3 onwards. Images reprinted from reference 22 by permission from Macmillan Publishers Ltd: Nature Medicine. (**D**) In the liver the type I collagen network (purple) visualized by second harmonic generation imaging was used to retrace the same position of multiple days. To show retracing, the images of day 1 and day 2 were given a false color (red or green respectively) and were merged. Yellow indicates colocalization. To quantify the amount of colocalization, the pixel intensity values of day 1 and day 2 in the merged image were displayed in a scatter plot. The Pearson correlation coefficient (*r*) was calculated and the non-colocalizing pixels were displayed in falce colors (red and blue) on top of the day 1 image displayed in gray. Scale bar, 20 μm. Image from reference 32, reprinted with permission from AAAS. (**E**) Dendra2 labeled tumor cells (green are non-photoswitched cells and red are photoswitched cells) imaged through a mammary imaging window. Images were taken 0, 6 and 24 h after photoswitching. Scale bar, 30 μm. Images reprinted from by reference 29, permission from Macmillan Publishers Ltd: Nature Methods.

for CIW imaging because it allows the animal to remain in its normal (upright) position (**Table 4**). For historical reasons, an upright microscope is also generally used to image the DSC, however inverted microscopes can also be used. In contrast, for the MIW and AIW, an inverted microscope is advisable because it reduces tissue movements caused by respiration.[83] To prevent imaging distortions due to tissue movement caused by respiration, the mouse and the imaging window should be fixed onto the microscope. Depending on the type of microscope (upright or inverted), different strategies are used to fix the imaging windows. **Figure 5A** shows an example of a custom-made imaging box that can be fixed on the stage of an inverted microscope. The mouse's head is introduced into a facemask that supplies isoflurane for sedation. An outlet ventilates the box, maintaining stable levels of anesthetics. In the lower part of the box an exchangeable metal plate is placed in which the imaging window is fixed.

Different metal plates are used for each type of window. A hole in the metal plate allows precise insertion of the MIW, AIW and CIW (**Fig. 5B and C**). Small magnets glued to the plate around an opening for imaging are used to fix the steel ring around the CIW (**Fig. 5C**). In case of an upright microscope, a stereotactic frame can be used to fix the CIW on the microscope. The DSC can be stably fixed to the stage by a special imaging mount (**Fig. 5D**). It should consist of a large central hole that permits imaging and three small holes that allow the bolts on the window to pass through. This imaging mount can be used on an upright or inverted microscope.[39]

Vital parameters control

A heat pad or thermal blankets underneath or above the animal can be used to maintain a body temperature of approximately 37 °C (**Table 4**).[6,41] It is important to realize that when a non-heated water objective is used, the imaged tissue will most

likely be cooled down by the much colder objective. For these experiments, we recommend use of a climate chamber that surrounds the whole microscope including the objective and microscope stage (**Fig. 5E**). Since the body temperature may change during the imaging session, it is recommended to measure the mouse temperature during the experiment by a rectal probe in order to adjust the heating. Additionally, the breath rate should be checked at least every half hour by visual inspection, but ideally continuously, and the isoflurane supply should be adjusted if irregular or abnormal breathing is observed. Accurate and continuous assessment of vital parameters can be assessed by non-invasive pulse oximetry (MouseOx system) (**Tables 1 and 4**). To avoid mouse dehydration during imaging, a maximum of 500 µl saline can be injected subcutaneously for short-term experiments (2–3 h) prior to imaging. For long-term experiments (>3 h), it is advisable to provide saline periodically by a subcutaneous infusion system (50–100 µl / hour).[6,12]

Repeat imaging

To image individual cells, groups of cells, or changes in tissue structure over multiple imaging sessions, several strategies have been developed to retrace imaging areas during successive microscope sessions. When the position of the imaging window relative to the microscope is fixed for successive imaging sessions, a motorized stage can be used to store and relocate the coordinates of imaging areas (**Fig. 6A**). Alternatively a numbered gridded coverslip on the imaging window can be used to provide the exact location of a previously imaged area (**Fig. 6B**).[32] Inherent landmarks such as the vascular networks and extracellular matrix structures can also be used to retrace the same region (**Fig. 6C and D**).[22] Vasculature can be imaged after intravenous injection of fluorescent molecules like fluorescently labeled dextrans or fluorescent red blood cells, or by using genetic mouse models. Extracellular matrix structures such as Type I collagen can be acquired by second harmonic generation microscopy (SHG).[32,84-86] Type I collagen has a highly organized structure that absorbs the energy of two photons and reflects a single photon with double energy and half the wavelength. However, in experimental systems that are highly dynamic (e.g., fast migrating and proliferating tumors such as gliomas), these above defined landmarks are not stable enough for retracing imaging areas. To allow for long-term cell tracing in dynamically changing tissues, photoconvertable fluorophores such as Dendra2 or Kaede can be used (**Fig. 6E**). The absorption and emission spectrum of these photoconvertable proteins shifts to longer wavelengths when it is illuminated with violet light. Single or groups of cells can be marked and traced over several days (**Fig. 6E**).[29] Another approach is the use of multicolored cells using the RGB marking or Confetti system.[87-89] Using these systems the progeny of tumor cells can be traced over time because cells of the same lineage have a similar color. If enough colors are used, the variation in colors allows for retracing of the same position.[11] Autofluorescence-based photo-tattoos are exogenous landmarks which can also be used to relocate an imaged area at a later time point. However, because this technique causes a change in the local microenvironment, fixation prior or immediately after placing the tattoo is advisable. Thus, it is most useful to retrace intravitally imaged areas

in cryosections.[59] For detailed advice on imaging implementation and troubleshooting consult **Table 4**.

Future Developments

Imaging windows are a valuable tool to gain optical access to tissues of interest. However, the surgical insertion and the presence of the imaging window will always have at least some influence on the imaged tissues. Ideally, one would use high-resolution intravital imaging techniques that provide direct optical access deep inside the animal without the requirement of an imaging window. Development of ultrasound based techniques that excite only those fluorophores within the focal plane, such as ultrasound-switchable fluorescence, may further advance non-invasive deep imaging while preserving high-resolution.[90,91] However, the effectiveness of this method in vivo still needs to be determined.

To our knowledge, all labs that utilize imaging windows anesthetize their animals while imaging, despite the change in tissue physiology that the anesthetics may cause. Interestingly, microobjectives have been developed that can be directly coupled to miniature microscopes (two-photon and epifluorescence) which can be carried by freely moving mice allowing in theory continuous imaging for months.[92,93] Although the resolution is currently one order lower than two-photon systems,[94] this may soon be overcome with new developments in micro-optics.[94]

Despite the advances in the field of imaging windows, not all organs can be imaged or are difficult to image for prolonged periods of time. For example, the organs that reside in the thorax (e.g., heart and lung) have traditionally been very difficult to image in living animals because of their anatomical location behind the ribs and due to respiratory movements. Recently, several labs made technical progress in this area and are now able to intravitally image these organs for a few hours. For the heart, a thoracotomy was performed to expose the organ. After combining a motion stabilizer tool with an image acquisition algorithm, imaging could be performed up to several hours.[95] For the lung, repeated whole body imaging measurements were performed after opening the chest wall to expose the organ and regulating lung ventilation.[96] The disadvantage of this approach is that it has limited resolution and it lacks a system to reduce respiratory motion. In contrast, Looney and colleagues have imaged the lung at subcellular resolution using a stabilizer device based on vacuum to prevent respiratory motion artifacts.[35] They could image the lung with high accuracy for up to 3 h. Permanent imaging windows for these thoracic organs would allow for repeated measurements over days and would be of great interest to, for example tumor biologists, to study lung metastases. Some of the specialized and distinct regions that are present in the brain have been difficult to image at high-resolution as well because they are beyond the imaging depth of a multi-photon microscope (<1.6 mm).[97] Therefore, guide tubes implanted in the brain have been used that allow repetitive insertion of micro-optical probes to visualize the pyramidal neurons in the hippocampus and blood flow dynamics in deep brain gliomas.[98] However, this approach

has several limitations, such as reduced imaging area (<1 mm) and resolution, alteration of brain architecture, and induction of glial response to the inserts.[98]

The currently used windows can also be further improved. For example, surgery-induced fibrosis is a problem of window surgeries, especially in the abdomen. Seprafilm Adhesion Barrier is used in the clinic to prevent fibrosis-induced adhesion of organs and has also yielded promising results during skin flap surgeries,[99-101] but has so far not been used for imaging window surgeries. Other areas of improvement should focus on extending the imaging time, reducing the weight of the windows without compromising the field of view and reducing exudate accumulation behind the window.

In conclusion, imaging windows are helpful tools to study individual and groups of cells in tumorigenic and healthy tissues by intravital microscopy. In this manuscript, we have established a framework for how to implant the most widely used imaging windows for cancer research, and described how to use them for imaging purposes.

References

1. Condeelis J, Weissleder R. In vivo imaging in cancer. Cold Spring Harb Perspect Biol 2010; 2:a003848; PMID:20861158; http://dx.doi.org/10.1101/cshperspect.a003848

2. Ritsma L, Ponsioen B, Van Rheenen J. Intravital imaging of cell signaling in mice. IntraVital 2012; 1:2-10; http://dx.doi.org/10.4161/intv.20802

3. Pittet MJ, Weissleder R. Intravital imaging. Cell 2011; 147:983-91; PMID:22118457; http://dx.doi.org/10.1016/j.cell.2011.11.004

4. Ellenbroek SI, van Rheenen J. Imaging hallmarks of cancer in living mice. Nat Rev Cancer 2014; 14:406-18; PMID:24854083; http://dx.doi.org/10.1038/nrc3742

5. Fein MR, Egeblad M. Caught in the act: revealing the metastatic process by live imaging. Dis Model Mech 2013; 6:580-93; PMID:23616077; http://dx.doi.org/10.1242/dmm.009282

6. Ewald AJ, Werb Z, Egeblad M. Preparation of mice for long-term intravital imaging of the mammary gland. Cold Spring Harb Protoc 2011; 2011:t5562; PMID:21285262; http://dx.doi.org/10.1101/pdb.prot5562

7. Garnett MJ, Edelman EJ, Heidorn SJ, Greenman CD, Dastur A, Lau KW, Greninger P, Thompson IR, Luo X, Soares J, et al. Systematic identification of genomic markers of drug sensitivity in cancer cells. Nature 2012; 483:570-5; PMID:22460902; http://dx.doi.org/10.1038/nature11005

8. Wyckoff J, Gligorijevic B, Entenberg D, Segall J, Condeelis J. High-resolution multiphoton imaging of tumors in vivo. Cold Spring Harb Protoc 2011; 2011:1167-84; PMID:21969629; http://dx.doi.org/10.1101/pdb.top065904

9. Zomer A, Beerling E, Vlug EJ, van Rheenen J. Real-time intravital imaging of cancer models. Clin Transl Oncol 2011; 13:848-54; PMID:22126727; http://dx.doi.org/10.1007/s12094-011-0745-3

10. Hefendehl JK, Wegenast-Braun BM, Liebig C, Eicke D, Milford D, Calhoun ME, Kohsaka S, Eichner M, Jucker M. Long-term in vivo imaging of β-amyloid plaque appearance and growth in a mouse model of cerebral β-amyloidosis. J Neurosci 2011; 31:624-9; PMID:21228171; http://dx.doi.org/10.1523/JNEUROSCI.5147-10.2011

11. Zomer A, Ellenbroek SI, Ritsma L, Beerling E, Vrisekoop N, Van Rheenen J. Intravital imaging of cancer stem cell plasticity in mammary tumors. Stem Cells 2013; 31:602-6; PMID:23225641; http://dx.doi.org/10.1002/stem.1296

12. Ritsma L, Ellenbroek SI, Zomer A, Snippert HJ, de Sauvage FJ, Simons BD, Clevers H, van Rheenen J. Intestinal crypt homeostasis revealed at single-stem-cell level by in vivo live imaging. Nature 2014; 507:362-5; PMID:24531760; http://dx.doi.org/10.1038/nature12972

13. Ravina F. De motu cerebri. Memoires de l'Academie des Sciences de Turin 1811; 20:61-93

14. Donders FC. De bewegingen der Hersenen en de veranderingen der vaatvulling van der "Pia Mater", ook bijgesloten onuitzetberen schedel regstreeks onderzocht. Nederlandsche Lancet 1850; 5:521-53

15. Forbes HS. The cerebral circulation: I. observation and measurement of pial vessels. Arch Neurol Psychiatry 1928; 19:751-61; http://dx.doi.org/10.1001/archneurpsyc.1928.02210110003001

16. Holtmaat A, Bonhoeffer T, Chow DK, Chuckowree J, De Paola V, Hofer SB, Hübener M, Keck T, Knott G, Lee WC, et al. Long-term, high-resolution imaging in the mouse neocortex through a chronic cranial window. Nat Protoc 2009; 4:1128-44; PMID:19617885; http://dx.doi.org/10.1038/nprot.2009.89

17. Grutzendler J, Kasthuri N, Gan WB. Long-term dendritic spine stability in the adult cortex. Nature 2002; 420:812-6; PMID:12490949; http://dx.doi.org/10.1038/nature01276

18. Mostany R, Portera-Cailliau C. A method for 2-photon imaging of blood flow in the neocortex through a cranial window. J Vis Exp 2008; 678; PMID:19066563; http://dx.doi.org/10.3791/678

19. Dreier JP, Victorov IV, Petzold GC, Major S, Windmüller O, Fernández-Klett F, Kandasamy M, Dirnagl U, Priller J. Electrochemical failure of the brain cortex is more deleterious when it is accompanied by low perfusion. Stroke 2013; 44:490-6; PMID:23287786; http://dx.doi.org/10.1161/STROKEAHA.112.660589

20. Miyauchi T, Wei EP, Povlishock JT. Therapeutic targeting of the axonal and microvascular change associated with repetitive mild traumatic brain injury. J Neurotrauma 2013; 30:1664-71; PMID:23796228; http://dx.doi.org/10.1089/neu.2013.2995

21. Murmu RP, Li W, Holtmaat A, Li JY. Dendritic spine instability leads to progressive neocortical spine loss in a mouse model of Huntington's disease. J Neurosci 2013; 33:12997-3009; PMID:23926255; http://dx.doi.org/10.1523/JNEUROSCI.5284-12.2013

22. Kienast Y, von Baumgarten L, Fuhrmann M, Klinkert WE, Goldbrunner R, Herms J, Winkler F. Real-time imaging reveals the single steps of brain metastasis formation. Nat Med 2010; 16:116-22; PMID:20023634; http://dx.doi.org/10.1038/nm.2072

23. Algire GH. An Adaptation of the Transparent-Chamber Technique to the Mouse. J Natl Cancer Inst 1943; 4:1-11

24. Sandison J. a new method for the microscopic study of living growing tissues by the introduction of a transparent chamber in the rabbit's ear. Anat Rec 1924; 28:281-7; http://dx.doi.org/10.1002/ar.1090280403

25. Lehr HA, Leunig M, Menger MD, Nolte D, Messmer K. Dorsal skinfold chamber technique for intravital microscopy in nude mice. Am J Pathol 1993; 143:1055-62; PMID:7692730

26. Alexander S, Koehl GE, Hirschberg M, Geissler EK, Friedl P. Dynamic imaging of cancer growth and invasion: a modified skin-fold chamber model. Histochem Cell Biol 2008; 130:1147-54; PMID:18987875; http://dx.doi.org/10.1007/s00418-008-0529-1

27. Sckell A, Leunig M. The Dorsal Skinfold Chamber: Studying Angiogenesis by Intravital Microscopy. Methods in Molecular Biology, Angiogenesis Protocols, Second Edition, Vol 467 Humana Press 2009

28. Menger MD, Vollmar B. In vivo analysis of microvascular reperfusion injury in striated muscle and skin. Microsurgery 1994; 15:383-9; PMID:7968463; http://dx.doi.org/10.1002/micr.1920150605

29. Kedrin D, Gligorijevic B, Wyckoff J, Verkhusha VV, Condeelis J, Segall JE, van Rheenen J. Intravital imaging of metastatic behavior through a mammary imaging window. Nat Methods 2008; 5:1019-21; PMID:18997781; http://dx.doi.org/10.1038/nmeth.1269

30. Shan S, Sorg B, Dewhirst MW. A novel rodent mammary window of orthotopic breast cancer for intravital microscopy. Microvasc Res 2003; 65:109-17; PMID:12686168; http://dx.doi.org/10.1016/S0026-2862(02)00017-1

31. Ritsma L, Steller EJ, Ellenbroek SI, Kranenburg O, Borel Rinkes IH, van Rheenen J. Surgical implantation of an abdominal imaging window for intravital microscopy. Nat Protoc 2013; 8:583-94; PMID:23429719; http://dx.doi.org/10.1038/nprot.2013.026

32. Ritsma L, Steller EJ, Beerling E, Loomans CJ, Zomer A, Gerlach C, Vrisekoop N, Seinstra D, van Gurp L, Schäfer R, et al. Intravital microscopy through an abdominal imaging window reveals a pre-micrometastasis stage during liver metastasis. Sci Transl Med 2012; 4:ra145; PMID:23115354; http://dx.doi.org/10.1126/scitranslmed.3004394

33. Farrar MJ, Bernstein IM, Schlafer DH, Cleland TA, Fetcho JR, Schaffer CB. Chronic in vivo imaging in the mouse spinal cord using an implanted chamber. Nat Methods 2012; 9:297-302; PMID:22266542; http://dx.doi.org/10.1038/nmeth.1856

34. Fenrich KK, Weber P, Hocine M, Zalc M, Rougon G, Debarbieux F. Long-term in vivo imaging of normal and pathological mouse spinal cord with subcellular resolution using implanted glass windows. J Physiol 2012; 590:3665-75; PMID:22641787; http://dx.doi.org/10.1113/jphysiol.2012.230532

35. Looney MR, Thornton EE, Sen D, Lamm WJ, Glenny RW, Krummel MF. Stabilized imaging of immune surveillance in the mouse lung. Nat Methods 2011; 8:91-6; PMID:21151136; http://dx.doi.org/10.1038/nmeth.1543

36. Presson RG Jr., Brown MB, Fisher AJ, Sandoval RM, Dunn KW, Lorenz KS, Delp EJ, Salama P, Molitoris BA, Petrache I. Two-photon imaging within the murine thorax without respiratory and cardiac motion artifact. Am J Pathol 2011; 179:75-82; PMID:21703395; http://dx.doi.org/10.1016/j.ajpath.2011.03.048

37. Gargiulo S, Greco A, Gramanzini M, Esposito S, Affuso A, Brunetti A, Vesce G. Mice anesthesia, analgesia, and care, Part I: anesthetic considerations in preclinical research. ILAR J 2012; 53:E55-69; PMID:23382271; http://dx.doi.org/10.1093/ilar.53.1.55

38. Mostany R, Portera-Cailliau C. A craniotomy surgery procedure for chronic brain imaging. J Vis Exp 2008; 680; PMID:19066562; http://dx.doi.org/10.3791/680

39. Palmer GM, Fontanella AN, Shan S, Hanna G, Zhang G, Fraser CL, Dewhirst MW. In vivo optical molecular imaging and analysis in mice using dorsal window chamber models applied to hypoxia, vasculature and fluorescent reporters. Nat Protoc 2011; 6:1355-66; PMID:21886101; http://dx.doi.org/10.1038/nprot.2011.349

40. Hart SR, Bordes B, Hart J, Corsino D, Harmon D. Unintended perioperative hypothermia. Ochsner J 2011; 11:259-70; PMID:21960760

41. Palmer GM, Fontanella AN, Shan S, Dewhirst MW. High-resolution in vivo imaging of fluorescent proteins using window chamber models. Methods Mol Biol 2012; 872:31-50; PMID:22700402; http://dx.doi.org/10.1007/978-1-61779-797-2_3

42. Ewald AJ, Werb Z, Egeblad M. Monitoring of vital signs for long-term survival of mice under anesthesia. Cold Spring Harb Protoc 2011; 2011:t5563; PMID:21285263; http://dx.doi.org/10.1101/pdb.prot5563

43. Iida H, Ohata H, Iida M, Watanabe Y, Dohi S. Isoflurane and sevoflurane induce vasodilation of cerebral vessels via ATP-sensitive K+ channel activation. Anesthesiology 1998; 89:954-60; PMID:9778013; http://dx.doi.org/10.1097/00000542-199810000-00020

44. Cavazzuti M, Porro CA, Biral GP, Benassi C, Barbieri GC. Ketamine effects on local cerebral blood flow and metabolism in the rat. J Cereb Blood Flow Metab 1987; 7:806-11; PMID:3121648; http://dx.doi.org/10.1038/jcbfm.1987.138

45. Akata T. General anesthetics and vascular smooth muscle: direct actions of general anesthetics on cellular mechanisms regulating vascular tone. Anesthesiology 2007; 106:365-91; PMID:17264732; http://dx.doi.org/10.1097/00000542-200702000-00026

46. Zuurbier CJ, Koeman A, Houten SM, Hollmann MW, Florijn WJ. Optimizing anesthetic regimen for surgery in mice through minimization of hemodynamic, metabolic, and inflammatory perturbations. Exp Biol Med (Maywood) 2014; 239:737-46; PMID:24668552; http://dx.doi.org/10.1177/1535370214524877

47. Matsuda Y, Ohsaka K, Yamamoto H, Natsume K, Hirabayashi S, Kounoike M, Inoue M. Comparison of newly developed inhalation anesthesia system and intraperitoneal anesthesia on the hemodynamic state in mice. Biol Pharm Bull 2007; 30:1716-20; PMID:17827727; http://dx.doi.org/10.1248/bpb.30.1716

48. Jenkins DE, Oei Y, Hornig YS, Yu SF, Dusich J, Purchio T, Contag PR. Bioluminescent imaging (BLI) to improve and refine traditional murine models of tumor growth and metastasis. Clin Exp Metastasis 2003; 20:733-44; PMID:14713107; http://dx.doi.org/10.1023/B:CLIN.0000006815.49932.98

49. Sabaa N, de Franceschi L, Bonnin P, Castier Y, Malpeli G, Debbabi H, Galaup A, Maier-Redelsperger M, Vandermeersch S, Scarpa A, et al. Endothelin receptor antagonism prevents hypoxia-induced mortality and morbidity in a mouse model of sickle-cell disease. J Clin Invest 2008; 118:1924-33; PMID:18382768; http://dx.doi.org/10.1172/JCI33308

50. Xu S, Jordan EK, Li W, Yang Y, Chesnick SA, Webster HD, Brocke S, Quigley L, McFarland HF, Frank JA. In vivo three-dimensional MR microscopy of mice with chronic relapsing experimental autoimmune encephalomyelitis after treatment with insulin-like growth factor-I. AJNR Am J Neuroradiol 1998; 19:653-8; PMID:9576650

51. Perkin RM, Resnik DB. The agony of agonal respiration: is the last gasp necessary? J Med Ethics 2002; 28:164-9; PMID:12042401; http://dx.doi.org/10.1136/jme.28.3.164

52. Tranquilli W, Thurmon J, Kurt A. Lumb & Jones' Veterinary Anesthesia and Analgesia, 4th Edition. Iowa: Blackwell Publishing, 2007.

53. van Versendaal D, Rajendran R, Saiepour MH, Klooster J, Smit-Rigter L, Sommeijer JP, De Zeeuw CI, Hofer SB, Heimel JA, Levelt CN. Elimination of inhibitory synapses is a major component of adult ocular dominance plasticity. Neuron 2012; 74:374-83; PMID:22542189; http://dx.doi.org/10.1016/j.neuron.2012.03.015

54. Schwenke DO, Cragg PA. Comparison of the depressive effects of four anesthetic regimens on ventilatory and cardiovascular variables in the guinea pig. Comp Med 2004; 54:77-85; PMID:15027622

55. Adam Y, Mizrahi A. Long-term imaging reveals dynamic changes in the neuronal composition of the glomerular layer. J Neurosci 2011; 31:7967-73; PMID:21632918; http://dx.doi.org/10.1523/JNEUROSCI.0782-11.2011

56. Badie B, Schartner JM, Paul J, Bartley BA, Vorpahl J, Preston JK. Dexamethasone-induced abolition of the inflammatory response in an experimental glioma model: a flow cytometry study. J Neurosurg 2000; 93:634-9; PMID:11014542; http://dx.doi.org/10.3171/jns.2000.93.4.0634

57. Essien BE, Kotiw M. Anti-inflammatory activity of hyperimmune plasma in a lipopolysaccharide-mediated rat air pouch model of inflammation. Inflammation 2012; 35:58-64; PMID:21213030; http://dx.doi.org/10.1007/s10753-010-9289-x

58. Condeelis J, Pollard JW. Macrophages: obligate partners for tumor cell migration, invasion, and metastasis. Cell 2006; 124:263-6; PMID:16439202; http://dx.doi.org/10.1016/j.cell.2006.01.007

59. Ritsma L, Vrisekoop N, van Rheenen J. In vivo imaging and histochemistry are combined in the cryosection labelling and intravital microscopy technique. Nat Commun 2013; 4:2366; PMID:23978961; http://dx.doi.org/10.1038/ncomms3366

60. de Visser KE, Coussens LM. The inflammatory tumor microenvironment and its impact on cancer development. Contrib Microbiol 2006; 13:118-37; PMID:16627962; http://dx.doi.org/10.1159/000092969

61. Hudson N, Balsitis M, Everitt S, Hawkey CJ. Angiogenesis in gastric ulcers: impaired in patients taking non-steroidal anti-inflammatory drugs. Gut 1995; 37:191-4; PMID:7557566; http://dx.doi.org/10.1136/gut.37.2.191

62. Kremers P, Duvivier J, Heusghem C. Pharmacokinetic studies of co-trimoxazole in man after single and repeated doses. J Clin Pharmacol 1974; 14:112-7; PMID:4813080; http://dx.doi.org/10.1002/j.1552-4604.1974.tb02300.x

63. Kaplan SA, Weinfeld RE, Abruzzo CW, McFaden K, Jack ML, Weissman L. Pharmacokinetic profile of trimethoprim-sulfamethoxazole in man. The Journal of infectious diseases 1973; 128:Suppl:547-55 p.

64. Bauer AW, Kirby WM, Sherris JC, Turck M. Antibiotic susceptibility testing by a standardized single disk method. Am J Clin Pathol 1966; 45:493-6; PMID:5325707

65. Cho CH, Sung HK, Kim KT, Cheon HG, Oh GT, Hong HJ, Yoo OJ, Koh GY. COMP-angiopoietin-1 promotes wound healing through enhanced angiogenesis, lymphangiogenesis, and blood flow in a diabetic mouse model. Proc Natl Acad Sci U S A 2006; 103:4946-51; PMID:16543381; http://dx.doi.org/10.1073/pnas.0506352103

66. Niinomi M. Recent research and development in titanium alloys for biomedical applications and healthcare goods. Sci Technol Adv Mater 2003; 4:445-54; http://dx.doi.org/10.1016/j.stam.2003.09.002

67. Osswald M, Winkler F. Insights into cell-to-cell and cell-to-blood-vessel communications in the brain: in vivo multiphoton microscopy. Cell Tissue Res 2013; 352:149-59; PMID:23435993; http://dx.doi.org/10.1007/s00441-013-1580-3

68. Shih AY, Mateo C, Drew PJ, Tsai PS, Kleinfeld D. A polished and reinforced thinned-skull window for long-term imaging of the mouse brain. J Vis Exp 2012; 3742; PMID:22433225; http://dx.doi.org/10.3791/3742

69. Dorand RD, Barkauskas DS, Evans TA, Petrosiute A, Huang AY. Comparison of intravital thinned skull and cranial window approaches to study CNS immunobiology in the mouse cortex. IntraVital 2014; 3:e29728; http://dx.doi.org/10.4161/intv.29728

70. Xu HT, Pan F, Yang G, Gan WB. Choice of cranial window type for in vivo imaging affects dendritic spine turnover in the cortex. Nat Neurosci 2007; 10:549-51; PMID:17417634; http://dx.doi.org/10.1038/nn1883

71. Yuan F, Salehi HA, Boucher Y, Vasthare US, Tuma RF, Jain RK. Vascular permeability and microcirculation of gliomas and mammary carcinomas transplanted in rat and mouse cranial windows. Cancer Res 1994; 54:4564-8; PMID:8062241

72. Winkler F, Kienast Y, Fuhrmann M, Von Baumgarten L, Burgold S, Mitteregger G, Kretzschmar H, Herms J. Imaging glioma cell invasion in vivo reveals mechanisms of dissemination and peritumoral angiogenesis. Glia 2009; 57:1306-15; PMID:19191326; http://dx.doi.org/10.1002/glia.20850

73. Brown E, Munn LL, Fukumura D, Jain RK. In Vivo Imaging of Tumors. Cold Spring Harb Protoc; 2010:pdb.prot5452-.

74. Moy AJ, White SM, Indrawan ES, Lotfi J, Nudelman MJ, Costantini SJ, Agarwal N, Jia W, Kelly KM, Sorg BS, et al. Wide-field functional imaging of blood flow and hemoglobin oxygen saturation in the rodent dorsal window chamber. Microvasc Res 2011; 82:199-209; PMID:21787792; http://dx.doi.org/10.1016/j.mvr.2011.07.004

75. Weigelin B. GJ B, P F. Intravital third harmonic generation microscopy of collective melanoma cell invasion: Principles of interface guidance and microvesicle dynamics. IntraVital 2012; 1:32-43; http://dx.doi.org/10.4161/intv.21223

76. A F. Guidelines for the Housing of Mice in Scientific Institutions Animal Research Review Panel 1 2012; Guideline 22.

77. Maeda A, DaCosta RS. Optimization of the dorsal skinfold window chamber model and multi-parametric characterization of tumor-associated vasculature. IntraVital 2014; 3:e27935; http://dx.doi.org/10.4161/intv.27935

78. Borgstrom P, Oh P, Czarny M, Racine B, Schnitzer JE. Co-implanting orthotopic tissue creates stroma microenvironment enhancing growth and angiogenesis of multiple tumors. F1000Res 2013; 2:129; PMID:24715954

79. Zhang SH, Zhang H, He HW, Li L, Li XQ, Zhang YP, Shao RG. Lidamycin up-regulates the expression of thymidine phosphorylase and enhances the effects of capecitabine on the growth and pulmonary metastases of murine breast carcinoma. Cancer Chemother Pharmacol 2013; 72:777-88; PMID:23975242; http://dx.doi.org/10.1007/s00280-013-2253-3

80. Shim JS, Matsui Y, Bhat S, Nacev BA, Xu J, Bhang HE, Dhara S, Han KC, Chong CR, Pomper MG, et al. Effect of nitroxoline on angiogenesis and growth of human bladder cancer. J Natl Cancer Inst 2010; 102:1855-73; PMID:21088277; http://dx.doi.org/10.1093/jnci/djq457

81. Gligorijevic B, Kedrin D, Segall JE, Condeelis J, van Rheenen J. Dendra2 photoswitching through the Mammary Imaging Window. J Vis Exp 2009; 1278; PMID:19578330; http://dx.doi.org/10.3791/1278

82. Janssen A, Beerling E, Medema R, van Rheenen J. Intravital FRET imaging of tumor cell viability and mitosis during chemotherapy. PLoS One 2013; 8:e64029; PMID:23691140; http://dx.doi.org/10.1371/journal.pone.0064029

83. Lee S, Vinegoni C, Feruglio PF, Weissleder R. Improved intravital microscopy via synchronization of respiration and holder stabilization. J Biomed Opt 2012; 17:96018-1; PMID:23085919; http://dx.doi.org/10.1117/1.JBO.17.9.096018

84. Perentes JY, McKee TD, Ley CD, Mathiew H, Dawson M, Padera TP, Munn LL, Jain RK, Boucher Y. In vivo imaging of extracellular matrix remodeling by tumor-associated fibroblasts. Nat Methods 2009; 6:143-5; PMID:19151720; http://dx.doi.org/10.1038/nmeth.1295

85. Friedl P. Dynamic imaging of cellular interactions with extracellular matrix. Histochem Cell Biol 2004; 122:183-90; PMID:15258769; http://dx.doi.org/10.1007/s00418-004-0682-0

86. Campagnola PJ, Millard AC, Terasaki M, Hoppe PE, Malone CJ, Mohler WA. Three-dimensional high-resolution second-harmonic generation imaging of endogenous structural proteins in biological tissues. Biophys J 2002; 82:493-508; PMID:11751336; http://dx.doi.org/10.1016/S0006-3495(02)75414-3

87. Coffey SE, Giedt RJ, Weissleder R. Automated analysis of clonal cancer cells by intravital imaging. Intravital 2013; 2:2; PMID:24349895; http://dx.doi.org/10.4161/intv.26138

88. Weber K, Thomaschewski M, Warlich M, Volz T, Cornils K, Niebuhr B, Täger M, Lütgehetmann M, Pollok JM, Stocking C, et al. RGB marking facilitates multicolor clonal cell tracking. Nat Med 2011; 17:504-9; PMID:21441917; http://dx.doi.org/10.1038/nm.2338

89. Snippert HJ, van der Flier LG, Sato T, van Es JH, van den Born M, Kroon-Veenboer C, Barker N, Klein AM, van Rheenen J, Simons BD, et al. Intestinal crypt homeostasis results from neutral competition between symmetrically dividing Lgr5 stem cells. Cell 2010; 143:134-44; PMID:20887898; http://dx.doi.org/10.1016/j.cell.2010.09.016

90. Yuan B, Uchiyama S, Liu Y, Nguyen KT, Alexandrakis G. High-resolution imaging in a deep turbid medium based on an ultrasound-switchable fluorescence technique. Appl Phys Lett 2012; 101:33703; PMID:22893732; http://dx.doi.org/10.1063/1.4737211

91. Pei Y, Wei MY, Cheng B, Liu Y, Xie Z, Nguyen K, Yuan B. High resolution imaging beyond the acoustic diffraction limit in deep tissue via ultrasound-switchable NIR fluorescence. Sci Rep 2014; 4:4690; PMID:24732947; http://dx.doi.org/10.1038/srep04690

92. Flusberg BA, Nimmerjahn A, Cocker ED, Mukamel EA, Barretto RP, Ko TH, Burns LD, Jung JC, Schnitzer MJ. High-speed, miniaturized fluorescence microscopy in freely moving mice. Nat Methods 2008; 5:935-8; PMID:18836457; http://dx.doi.org/10.1038/nmeth.1256

93. Piyawattanametha W, Cocker ED, Burns LD, Barretto RP, Jung JC, Ra H, Solgaard O, Schnitzer MJ. In vivo brain imaging using a portable 2.9 g two-photon microscope based on a microelectromechanical systems scanning mirror. Opt Lett 2009; 34:2309-11; PMID:19649080; http://dx.doi.org/10.1364/OL.34.002309

94. Barretto RP, Messerschmidt B, Schnitzer MJ. In vivo fluorescence imaging with high-resolution microlenses. Nat Methods 2009; 6:511-2; PMID:19525959; http://dx.doi.org/10.1038/nmeth.1339

95. Lee S, Vinegoni C, Feruglio PF, Fexon L, Gorbatov R, Pivoravov M, Sbarbati A, Nahrendorf M, Weissleder R. Real-time in vivo imaging of the beating mouse heart at microscopic resolution. Nat Commun 2012; 3:1054; PMID:22968700; http://dx.doi.org/10.1038/ncomms2060

96. Kimura H, Hayashi K, Yamauchi K, Yamamoto N, Tsuchiya H, Tomita K, Kishimoto H, Bouvet M, Hoffman RM. Real-time imaging of single cancer-cell dynamics of lung metastasis. J Cell Biochem 2010; 109:58-64; PMID:19911396

97. Kobat D, Horton NG, Xu C. In vivo two-photon microscopy to 1.6-mm depth in mouse cortex. J Biomed Opt 2011; 16:106014; PMID:22029361; http://dx.doi.org/10.1117/1.3646209

98. Barretto RP, Ko TH, Jung JC, Wang TJ, Capps G, Waters AC, Ziv Y, Attardo A, Recht L, Schnitzer MJ. Time-lapse imaging of disease progression in deep brain areas using fluorescence microendoscopy. Nat Med 2011; 17:223-8; PMID:21240263; http://dx.doi.org/10.1038/nm.2292

99. Tanaka K, Morimoto Y, Toiyama Y, Matsushita K, Kawamura M, Koike Y, Okugawa Y, Inoue Y, Uchida K, Araki T, et al. In vivo time-course imaging of tumor angiogenesis in colorectal liver metastases in the same living mice using two-photon laser scanning microscopy. J Oncol 2012; 2012:265487; PMID:22131993; http://dx.doi.org/10.1155/2012/265487

100. Tanaka K, Okigami M, Toiyama Y, Morimoto Y, Matsushita K, Kawamura M, Hashimoto K, Saigusa S, Okugawa Y, Inoue Y, et al. In vivo real-time imaging of chemotherapy response on the liver metastatic tumor microenvironment using multiphoton microscopy. Oncol Rep 2012; 28:1822-30; PMID:22923070

101. Kotsuma M, Parashurama N, Smith BR, Wo J, Ito K, Gambhir SS. Nondestructive, serial in vivo imaging of a tissue-flap using a tissue adhesion barrier: Applications for IVM imaging in the mammary fat pad and lymph node. IntraVital 2012; 1:69-76; http://dx.doi.org/10.4161/intv.21769

102. Moeller BJ, Cao Y, Li CY, Dewhirst MW. Radiation activates HIF-1 to regulate vascular radiosensitivity in tumors: role of reoxygenation, free radicals, and stress granules. Cancer Cell 2004; 5:429-41; PMID:15144951; http://dx.doi.org/10.1016/S1535-6108(04)00115-1

103. Vinegoni C, Lee S, Feruglio PF, Weissleder R. Advanced Motion Compensation Methods for Intravital Optical Microscopy. IEEE J Sel Top Quantum Electron 2014; 20; PMID:24273405; http://dx.doi.org/10.1109/JSTQE.2013.2279314

104. Lee S, Vinegoni C, Sebas M, Weissleder R. Automated motion artifact removal for intravital microscopy, without a priori information. Sci Rep 2014; 4:4507; PMID:24676021; http://dx.doi.org/10.1038/srep04507